American Mineralogist, Volume 84, pages 733–745, 1999

Solubility and stability of beryl in granitic melts

JOSEPH M. EVENSEN,[1,2,*] DAVID LONDON,[1] AND RICHARD F. WENDLANDT[2]

[1]School of Geology and Geophysics, University of Oklahoma, 100 East Boyd Street, Norman, Oklahoma 73019, U.S.A.
[2]Department of Geology and Geological Engineering, Colorado School of Mines, 1516 Illinois Street, Golden, Colorado 80401, U.S.A.

ABSTRACT

Beryllium contents of granitic melts at saturation in beryl (± chrysoberyl, phenakite, or quartz) have been determined by forward- and reverse-direction experiments at 650–850 °C and 200 MPa using natural beryl or the compositionally equivalent mixture of phenakite + alumina + quartz added to metaluminous haplogranite, peraluminous haplogranite, and macusanite (a peraluminous Li, B, F, and P enriched rhyolite obsidian from Macusani, Peru). Chrysoberyl coexists with beryl ± quartz in moderately to strongly peraluminous systems (ASI approximately ≥1.05); the assemblage phenakite + beryl + chrysoberyl is stable in silica-undersaturated bulk compositions. The BeO content of the melts, which ranged between 0.03–0.40 wt%, varies principally with temperature (the solubility of beryl falls with decreasing T) and with the activity product of beryl, $(a_{BeO})^3(a_{Al_2O_3})(a_{SiO_2})^6$. Beryllia contents are lowest in strongly peraluminous and quartz-saturated haplogranite melts; however, the highest BeO content measured in glass products occurs for the strongly peraluminous macusanite at 850 °C (4016 ppm); we infer that the greater solubility of beryl in macusanite melt results from melt speciation reactions involving Li, F, B, and P. For all bulk compositions studied, the BeO content of melt projects to a narrow range of similar values at low T, near the solidus of haplogranite. Thus, metaluminous to peraluminous granitic magmas with and without common volatile and fluxing components will, if cooled to subsolidus temperatures, have similarly low BeO requirements for beryl saturation. The small BeO content of melt near the solidus of haplogranite results in a minor (10 °C) depression of the freezing point. Compared to Be-free haplogranite melt, the mean melt composition at the beryl-saturated granite minimum shifts slightly toward quartz. Beryl is common in peraluminous granitic rocks in part because lower BeO contents are required to saturate these melts in beryl, and possibly because these melts acquire higher BeO contents by mica melting reactions at their sources. Beryl is also a common constituent of border-facies assemblages in granitic pegmatite dikes, regardless of their ASI values. This early crystallization of beryl results from the low BeO content required to saturate *any* granitic melt in beryl at the low-T environments in which pegmatite dikes solidify.

INTRODUCTION

Despite its low crustal abundance (2.8 ppm, Taylor 1964), beryllium forms 90 minerals in which Be is an essential structural component (Fleischer and Mandarino 1995; E.S. Grew, personal communication, 1998). Among these, beryl ($Be_3Al_2Si_6O_{18}$) is by far the most common. Beryl (Brl) occurs principally in granitic pegmatites, but it is also found in topaz rhyolite, associated hydrothermal deposits (e.g., veins, greisens), and other metamorphic rocks (e.g., gneiss), and less commonly in leucogranites (see Beus 1966 for summaries of occurrences). The occurrence of beryl rather than other Be-silicates in granitic pegmatites stems from its stability relations in quartz-saturated portions of the system BeO-Al_2O_3-SiO_2-H_2O (Burt 1978; Franz and Morteani 1981; Barton 1986; Cemic et al. 1986), in which divariant assemblages containing beryl + quartz occur over the range of moderate pressures and temperatures pertinent to the magmatic consolidation of pegmatites (e.g., Černý 1991a). The topologies (Fig. 1) predict three stability fields containing three-phase assemblages among beryl, phenakite (Be_2SiO_4), chrysoberyl ($BeAl_2O_4$), and quartz. Beryl-bearing pegmatites are commonly peraluminous in composition, and therefore the mineral assemblage beryl + chrysoberyl + quartz may be relevant to the magmatic portion of their crystallization. In natural systems, however, the back reaction of chrysoberyl (Cbr) via:

$$\underset{\text{chrysoberyl}}{3\ BeAl_2O_4} + \underset{\text{potassium feldspar}}{2\ KAlSi_3O_8} + \underset{\text{quartz}}{6\ SiO_2} =$$

$$\underset{\text{beryl}}{Be_3Al_2Si_6O_{18}} + \underset{\text{muscovite}}{2\ KAl_3Si_3O_{10}(OH)_2} \qquad (1)$$

tends to leave beryl as the predominant Be mineral. The assemblage Cbr + Brl + Phn (phenakite) is not anticipated in quartz-saturated systems such as granitic pegmatites, but is of interest because it contains all of the important "magmatic" Be phases.

The solubilities of Be minerals in granitic melts are not known, nor are the effects of Be on the liquidus or solidus temperatures. Addition of BeO is known to increase the viscosity of haplogranite melt at temperatures less than 1000 °C (Hess et al. 1995). The contrasting effects on viscosity of Be vs. F, B, and other common non-haplogranite components of pegmatite-forming magmas (Dingwell et al. 1996) implies that the interactions and consequences of Be are fundamentally different.

*E-mail: jevensen@ou.edu

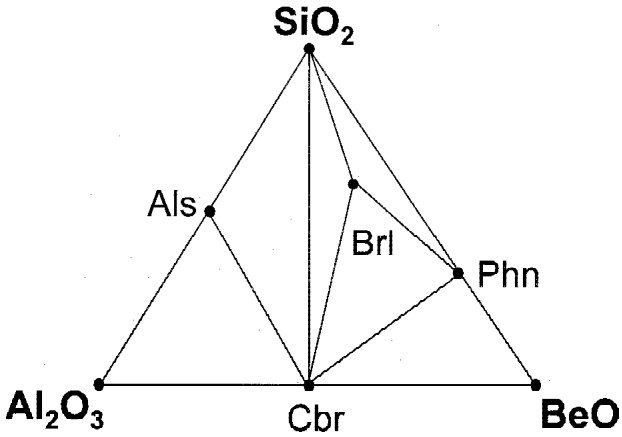

FIGURE 1. Proposed phase relations in the system BeO-Al_2O_3-SiO_2-H_2O at the moderate *P-T* conditions investigated in this study (685–850 °C, 200 MPa). The tie line Cbr-Qtz is stable here but is predicted to be replaced by Als-Brl (or equivalent) at lower temperatures (Barton 1986). Bertrandite [$Be_4Si_2O_7(OH)_2$] and euclase [$BeAlSiO_4(OH)$], not shown here, also become stable at lower temperatures. Mineral assemblages are from Burt (1978) and Barton (1986).

PURPOSE OF THIS STUDY

Beryllium mineral stabilities in the system BeO-Al_2O_3-SiO_2-H_2O (BASH system: Burt 1978; Barton 1986) are well defined, but the solubilities (especially with regard to BeO) of these minerals in granitic melt, and the effects, if any, of BeO on solidus or liquidus relations are unknown. Because beryl is such a widespread phase in granitic pegmatites, it is necessary to consider its significance in terms of the overall characterization of pegmatitic melts and their properties (London 1996; Dingwell et al. 1996).

In this paper, we define the BeO contents of beryl-saturated melts as functions of temperature (650–850 °C) and melt composition at 200 MPa (H_2O). Starting metaluminous, peraluminous, and strongly peraluminous granitic systems were chosen to bracket the compositional range of beryl-bearing pegmatites. The effects of BeO (concentration buffered by beryl saturation) on the freezing point and composition of the minimum haplogranitic melt were also determined. We utilize these results to explain several aspects of the occurrence of beryl in granitic pegmatites.

METHODOLOGY

Experimental methods

Starting materials. Beryl saturation was evaluated using three granitic compositions (Table 1): a metaluminous haplogranite mixture (HGS4; $Ab_{39}Or_{27}Qz_{34}$), a peraluminous haplogranite mixture (HGS5; $Ab_{37}Or_{24}Qz_{34}Cor_5$), and the peraluminous Li, B, P, and F-rich rhyolite obsidian (MAC) from Macusani, Peru (partial analysis in Table 1; see London et al. 1988 for a complete analysis). The low solidus temperature of macusanite (London et al. 1989) permitted investigations below the solidus of less-evolved haplogranite compositions and served as an analog to phase relations involving beryl in typical Li-rich pegmatites. HGS4 was formulated from natural

TABLE 1. Glass compositions of mixes (no other minerals added)

Powder	HGS4		HGS5		MAC*
No. of analyses	20		11		
	oxide wt%				
SiO_2	72.32	(0.25)	71.93	(0.32)	72.32
TiO_2	<0.02		<0.02		<0.02
B_2O_3	nd		nd		0.62
Al_2O_3	11.65	(0.39)	13.44	(0.11)	15.63
FeO	0.00		0.00		0.52
MnO	<0.06		<0.06		<0.06
MgO	<0.02		<0.02		<0.02
CaO	0.02	(0.02)	0.02	(0.02)	0.23
Li_2O	nd		nd		0.34
Na_2O	4.14	(0.20)	4.00	(0.12)	4.10
K_2O	4.50	(0.14)	3.92	(0.09)	3.53
P_2O_5	nd		nd		0.58
F	nd		nd		1.30
H_2O	nd		nd		0.30
Total†	92.63		93.31		99.47
H_2O diff	7.37		6.69		
	CIPW normative %				
Qtz	33.5		36.1		36.8
Or	28.7		24.8		21.5
Ab	37.8		36.3		33.1
An					
Hy					1.0
Cor			2.8		6.2
Ilm					
Ap					1.4
ASI†	1.00		1.24		1.33

Note: MAC ASI value accounts for Li_2O.
* Partial analysis, from London et al. (1988).
† Totals are low because they do not account for H_2O contents of glass.
‡ ASI = mol Al_2O_3/(alkali oxides + alkaline earth oxides).

mineral phases (albite, Copelinha, Brazil; orthoclase, St. Gotthard, Switzerland; semiconductor-grade quartz, Spruce Pine, North Carolina, U.S.A.; see Table 2) to approximate the hydrous ternary minimum melting composition (Tuttle and Bowen 1958) at 200 MPa (H_2O). HGS5 was derived from HGS4 by addition of activated amorphous Al_2O_3, which was created by decomposing synthetic gibbsite in air at 400 °C for 5 h.

Gem-quality beryl (Volodarsk, Ukraine) and gem-quality phenakite (Espirito Santo, Brazil) were added to granitic mixes as sources of beryllium (Table 2). Utilizing the reaction

$$\underset{\text{beryl}}{2\ Be_3Al_2Si_6O_{18}} = \underset{\text{phenakite}}{3\ Be_2SiO_4} + \underset{\text{alumina}}{2\ Al_2O_3} + \underset{\text{quartz}}{9\ SiO_2} \qquad (2)$$

the saturation of melt with beryl was approached by addition of (1) beryl and (2) the compositionally equivalent but reactive mixture of phenakite + alumina + quartz (cf. Fig. 4a). Each Be source was added separately to HGS4, HGS5, and MAC. These compositions produced a range of ASI values (ASI = alumina saturation index, mol alumina/$\sum$alkali oxides + alkaline earth oxides) up to saturation in chrysoberyl, the most aluminous crystalline phase stable with beryl-bearing assemblages (Fig. 1). Sufficient quartz was added to HGS4 and HGS5 (referred to by "+ Qtz" in the bulk composition) to maintain quartz-saturation of melt between 700–850 °C at 200 MPa, thereby fixing a_{SiO_2} in melt.

Each starting composition contained 75 wt% haplogranite or macusanite and 25 wt% beryl (e.g., referred to as HGS4 + Brl) or the phenakite-bearing mixture (products of Eq. 2; e.g., referred to as HGS4 + Phn mix). A slight excess of doubly distilled deionized water needed to saturate melt at these condi-

TABLE 2. Starting materials

	Added Minerals*				
	albite	orthoclase	quartz	beryl	phenakite
No. of analyses	5	20	6	5	5
			oxide wt%		
SiO_2	68.82 (0.16)	64.95 (0.36)	99.99 (0.03)	66.00 (0.20)	54.34 (0.32)
TiO_2	nd	nd	nd	0.06 (0.02)	0.00
Al_2O_3	19.76 (0.05)	18.76 (0.14)	nd	19.24 (0.10)	0.00
FeO†	nd	nd	nd	0.48 (0.13)	0.03 (0.02)
MnO	nd	nd	nd	0.00 (0.00)	0.00
BeO	nd	nd	nd	14.09‡	46.17§ (0.99)
MgO	nd	nd	nd	0.00	0.00
CaO	0.07 (0.01)	0.01 (0.02)	nd	0.00	0.00
BaO	0.06 (0.05)	0.32 (0.04)	nd	0.03 (0.03)	0.14 (0.01)
Na_2O	11.59 (0.04)	1.21 (0.07)	nd	0.08 (0.01)	0.00
K_2O	0.23 (0.02)	14.84 (0.07)	nd	0.03 (0.03)	0.00
Total	100.53	100.09	99.99	85.91II	100.68

Note: Numbers in parantheses represent 1 standard deviation of the mean.
* Albite, Copelinha, Minas Gerias, Brazil; orthoclase, St. Gotthard, Switzerland; quartz, ultrahigh purity, Feldspar Corp., Spruce Pine, N.C., U.S.A.; beryl, Volodarsk, Ukraine; phenakite, Espirito Santo, Minas Gerais, Brazil.
† Total iron as FeO.
‡ Calculated by difference.
§ Analyzed by secondary ion mass spectrometry.
II Not including BeO.

tions was added to each charge (target amount was 10 wt% H_2O for HGS4 and HGS5 runs and 12 wt% H_2O for macusanite runs). Consequently, each bulk composition contained ~3.0 wt% BeO.

Preparation of charges. Gold and platinum capsules (3 × 20 mm) were cleaned by soaking overnight in HF and by boiling for several hours in HNO_3. Even so, the capsules still contained remnants of the extrusion lubricants used in the fabrication of the tubing, and these were removed with foam swabs.

Phases used to prepare starting compositions were ground in an agate mortar under ethanol to a mean grain size of 10 mm and dried in air at 140 °C. Powdered components were combined by additional grinding and drying at 140 °C, and mixes were homogenized overnight in a tumbling mill. Water was loaded first, followed by powder mixes, into capsules (with powder mix confined to a central 5 × 3 mm portion of the capsule), which were sealed by arc welding. Sealed capsules were stored in a drying oven at 140 °C for several hours to homogenize contents. Capsules were checked for leaks before and after welding, and again after storage in a drying oven.

Experimental equipment. Experiments were pressurized cold in Rene-41 and NIMONIC-105 cold-seal reaction vessels using water plus trace Immunol as the pressure medium. For near-solidus melting experiments, Be-bearing and Be-absent (control) charges were loaded together into the same vessel. Pressure was measured with factory-calibrated Heise bourdon tube gauges, with fluctuations of <3 MPa over the course of experiments. Experiments were performed at the Colorado School of Mines (CSM), Golden, Colorado, and the University of Oklahoma (OU), Norman, Oklahoma. Experiment durations varied from 2–6 weeks.

Furnace temperature was controlled by Chromel-Alumel (OU) and Pt (CSM) wire resistance. Temperature was monitored by internal (OU) and external (CSM) Chromel-Alumel thermocouples, with estimated total error of ±5 °C (OU) and ±10 °C (CSM). Experiments were quenched isobarically in a compressed air jet (5–15 °C/s). The fugacity of oxygen within capsules was regulated by diffusion of H_2 across the metal capsule; the f_{O_2} of the pressure medium is slightly below NNO (Huebner 1971). Following quench, capsules were weighed to check for leaks, punctured and the presence of free water was recorded. Punctured capsules were placed in a drying oven, and following dehydration, capsules were reweighed to verify loss of free water. All capsules gain weight during experiments by diffusion of Ni-metal (from vessels and filler rods) into precious metal capsule walls; none of the experimental products reported here, however, suffered contamination by Ni.

Experimental pathways. Prograde (forward-direction) and retrograde (reverse-direction) thermal pathways were implemented in experiments to constrain melt compositions. Forward-direction experiments mostly entailed crystal melting, whereas reverse-direction runs promoted crystallization by utilizing high temperature to oversaturate the melt in components of interest relative to their melt concentrations at the final temperature of the experiment. Forward-direction experiments were taken directly to the temperature of interest, whereas reverse-direction experiments were preconditioned at a higher temperature (typically 850 °C for 6–10 days), quenched isobarically to room temperature, and then raised in a forward fashion to the final target temperature.

Analytical methods

Experimental products were inspected visually, petrographically, by oil immersion, and using backscattered electron imaging (BSEI) and energy-dispersive X-ray analysis (EDXA). Criteria for determination of water saturation included (1) free water upon opening capsules; (2) vapor dimples on glass surfaces; (3) presence of vapor deposits; (4) compositional homogeneity of melt (glass); and (5) phase relations of run products.

Quantitative electron probe microanalysis (QEPMA). All major and minor element oxide constituents of mineral and glass products, except beryllium, were analyzed using wavelength-dispersive spectrometry on a Cameca SX-50 electron microprobe at OU and a JEOL 8900 electron microprobe at the USGS, Denver, Colorado. QEPMA utilized crystalline and glass standards with TAP, PET, LIF, and layered composite PC1(OU) and LDEB (USGS) diffraction "crystals." Operating conditions

for hydrous glass analyses included a two-beam condition (2 nA and 20 nA regulated current) with a 20 μm spot size, in which Na and Al were analyzed first to inhibit beam-induced migration effects (Morgan and London 1996). Analyses of minerals were conducted at 20 nA, 20 kV (OU), and 15 kV (USGS), and a spot size of 3–5 μm. Counting times for all elements varied between 20 and 30 s. Data were reduced using PAP (Pouchou and Pichoir 1985) and CITZAF (Armstrong 1989) matrix correction routines at OU and the USGS, respectively. Detection levels, taken at 3σ above mean background, were <500 ppm for most elements. QEPMA at the USGS using the LDEB crystal (*d*-spacings optimized for boron analysis), calibrated against a Be-metal standard, checked for alloying of Be into Au or Pt capsules. At a detection limit of 210 ppm Be (Evensen and Meeker 1997), no Be contamination of capsule walls was found.

Ion microprobe-secondary ion mass spectrometry. Three Be-bearing granitic glasses were synthesized as standards for the analysis of experimental run glasses using secondary ion mass spectrometry (SIMS). These standards were formulated using powdered additions of phenakite to macusanite (Barnes et al. 1970; London et al. 1989) to produce glasses containing 0.6, 1.1, and 3.3 wt% BeO. Each mixture was sealed by arc welding and melted in platinum capsules (5 × 25 mm) at 1550 °C using a DelTech 1 atm furnace (CSM). Products were quenched, crushed and ground in agate, sealed, and reheated for at least three cycles to achieve homogeneity. No crystalline phases were found among the products. Beryllium concentrations were checked, following a four-acid dissolution technique (modified after Crock et al. 1983) and dilution, by inductively coupled plasma–atomic emission spectrometry (ICP-AES) at CSM. The homogeneity of major and minor elements in glass was assessed by QEPMA and SIMS. Homogeneity and correspondence of SIMS vs. ICP results are both excellent (Fig. 2).

Beryllium was analysed by SIMS using a Cameca Instruments IMS 4f operated by the University of New Mexico and Sandia National Laboratories at Albuquerque, New Mexico. An isotopically filtered $^{16}O^-$ primary beam was accelerated through a potential of 12.5 kV, with a beam current of 20 nA and a focused spot of 20–25 μm. The beam initially was rastered over an area of about 100 × 100 μm to expose sample surface. Sputtered secondary ions were accelerated through a potential of 4.5 kV and filtered using an energy offset of –100 V to eliminate isobaric interferences. Individual analyses consisted of 200 s of data acquisition, which included 20 repeated scan cycles over the stepped mass sequence ^{9}Be, ^{30}Si, and $^{7.75}$background, to achieve precision of at least 3% (average internal precision was 1.1%). Absolute concentrations were determined using empirical ratios for $^{30}Si^+$ (which in turn was set in proportion to the Si content derived from QEPMA). Calibration utilized the near-zero Be content of a natural rhyolite standard in addition to the three synthesized Be-rich glasses to bracket the Be contents of unknowns (Fig. 2). Total internal and external precision (ICP) of BeO analyses of glass was <3.9%. Data were acquired in two sessions, 13 months apart. Between these sessions, SIMS results were highly reproducible (±5–10 ppm).

Interferences between ^{9}Be (9.01219 amu) and $^{27}Al^{3+}$ (8.99384 amu) were distinguished by high resolution mass scans of standards (Fig. 3). Corrections were calculated in proportion to Al_2O_3 contents of glasses and applied, totaling approximately less 7 ppm BeO for unknowns.

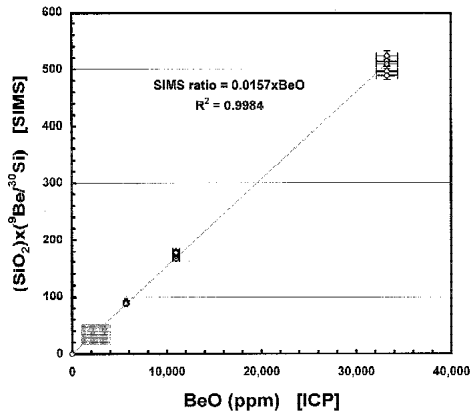

FIGURE 2. BeO standard calibration for analysis by SIMS. The standardized curve is calibrated among QEPMA, ICP-AES, and SIMS raw data. Twenty six data points are shown from analyses of 3 Be-rich glasses (containing 0.57, 1.10, and 3.33 wt% BeO) synthesized from the Macusani rhyolite obsidian and the DM0 rhyolite standard (UNM/Sandia SIMS Facility), which contains 10.8 ppm BeO. The shaded region depicts the range of values for experiments in this study.

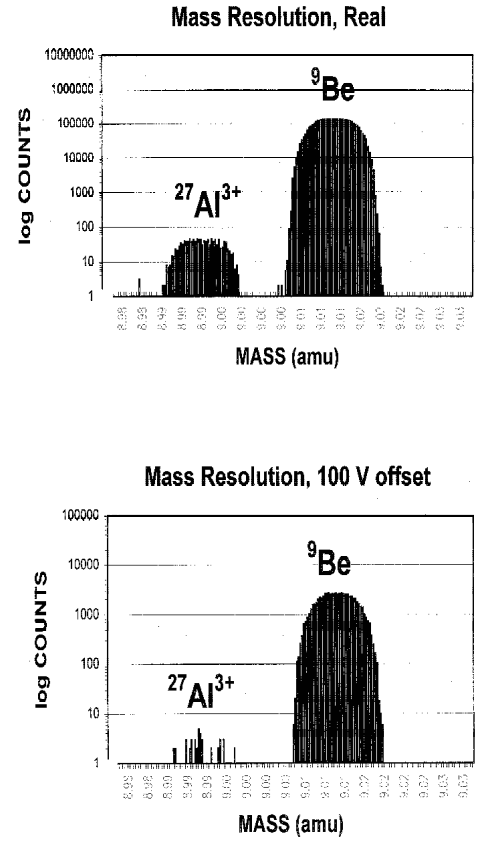

FIGURE 3. Mass scans between 8.980 and 9.030 amu utilizing SIMS. Beryllium values of unknowns at the conditions of analysis (20 nA), however, required correction for $^{23}Al^{3+}$ interferences. Applied corrections, calibrated against standards, amounted to ~7 ppm less BeO for glasses. Comparison between the plots illustrates the purpose of the imposed energy offset.

TABLE 3a. Glass compositions of HGS4 run products—HGS4 + Brl experiments

Run no.	BE-53	BE-18	BE-22	BE-54	BE-55	BE-14
Temp. (°C)–Path*	700-R	750-F	750-R	800-F	800-R	850-F
t (h) at T_{final}	720	980	816	672	600	144
Mineral products†	Brl, Phn	Brl	Brl	Brl	Brl, Phn	Brl
No. of analyses	12	5	5	12	12	12
			weight percent			
SiO_2	71.71 (0.61)	71.95 (0.86)	73.53 (0.34)	72.31 (0.30)	71.49 (0.42)	72.83 (0.39)
TiO_2	0.01 (0.01)	0.01 (0.01)	0.01 (0.01)	0.01 (0.01)	0.01 (0.01)	nd
Al_2O_3	11.96 (0.16)	11.60 (0.37)	11.89 (0.15)	12.09 (0.22)	12.21 (0.21)	12.12 (0.22)
FeO	0.03 (0.01)	0.03 (0.01)	0.03 (0.01)	0.03 (0.01)	0.04 (0.01)	nd
MnO	0.01 (0.01)	0.00 (0.00)	0.00 (0.00)	0.00 (0.00)	0.00 (0.00)	nd
BeO (ppm)	1118 (2)	1463 (16)	1606 (18)	2351 (3)	2146 (4)	3136 (35)
MgO	0.00 (0.00)	0.00 (0.00)	0.00 (0.00)	0.01 (0.00)	0.01 (0.01)	nd
CaO	0.04 (0.02)	0.03 (0.02)	0.04 (0.02)	0.05 (0.02)	0.05 (0.05)	0.01 (0.01)
BaO	0.12 (0.05)	0.09 (0.04)	0.10 (0.02)	0.11 (0.03)	0.10 (0.04)	nd
Na_2O	3.96 (0.15)	4.00 (0.10)	3.99 (0.04)	4.05 (0.15)	3.97 (0.14)	3.87 (0.16)
K_2O	4.05 (0.09)	4.33 (0.15)	4.23 (0.08)	3.99 (0.12)	4.09 (0.10)	4.32 (0.10)
P_2O_5	0.02 (0.01)	0.19 (0.05)	0.15 (0.09)	0.02 (0.01)	0.02 (0.01)	nd
F	0.03 (0.03)	0.11 (0.07)	0.13 (0.09)	0.06 (0.05)	0.03 (0.03)	nd
F = O	–0.01 (0.01)	–0.05 (0.03)	–0.05 (0.04)	–0.02 (0.02)	–0.01 (0.01)	nd
Total	92.04	92.44	94.21	92.95	92.22	93.46
H_2O diff	7.96	7.56	5.79	7.05	7.78	6.54
			CIPW normative %			
Ab	36.5	36.8	36.1	37.1	36.6	35.2
Or	26.1	27.9	26.7	25.5	26.3	27.4
Qtz	36.2	35.0	36.5	36.2	35.7	36.3
Cor	1.2	0.4	0.8	1.2	1.4	1.2
ASI	1.05 (0.03)	0.97 (0.01)	1.00 (0.01)	1.00 (0.04)	1.02 (0.03)	0.98 (0.03)

Note: BeO in included in calculated ASI values.
* F = forward run path; R = reversed run path.
† Crystalline run products are shown. Brl = beryl; Cbr = chrysoberyl; Phn = phenakite; Afs = alkali feldspar; Qtz = quartz. Relict phases interpreted to be metastable are shown in parentheses.

TABLE 3b. Glass compositions of HGS4 run products—HGS4 + Brl + Qtz experiments

Run no.	BE-64	BE-66	BE-68	BE-70	BE-72	BE-74	BE-76
Temp. (°C)–Path	700-F	700-R	750-F	750-R	800-F	800-R	850-F
t (h) at T_{final}	720	700	720	792	408	408	168
Mineral products	Brl, Qtz, Afs	Brl, Qtz	Brl, Qtz	Brl, Qtz	Brl, Qtz	Brl, Qtz	Brl, Qtz
No. of analyses	13	12	12	12	12	12	12
				weight percent			
SiO_2	72.56 (0.77)	73.82 (0.52)	73.97 (0.49)	74.64 (1.05)	76.39 (0.55)	76.74 (0.34)	77.77 (0.62)
Al_2O_3	11.44 (0.23)	11.25 (0.21)	10.73 (0.17)	10.67 (0.20)	9.85 (0.12)	9.67 (0.19)	9.00 (0.12)
BeO (ppm)	1280 (10)	1247 (9)	1589 (8)	1457 (9)	2117 (7)	2087 (7)	2569 (9)
CaO	0.03 (0.02)	0.03 (0.02)	0.03 (0.03)	0.04 (0.02)	0.02 (0.02)	0.02 (0.02)	0.02 (0.02)
Na_2O	3.71 (0.10)	3.61 (0.11)	3.45 (0.08)	3.40 (0.11)	3.12 (0.10)	3.09 (0.07)	2.75 (0.11)
K_2O	4.05 (0.10)	4.08 (0.07)	3.79 (0.07)	3.81 (0.09)	3.46 (0.06)	3.41 (0.08)	3.13 (0.11)
Total	91.92	92.91	92.13	92.71	93.05	93.14	92.93
H_2O diff	8.08	7.09	7.87	7.29	6.95	6.86	7.07
				CIPW normative %			
Ab	34.2	32.9	31.8	31.1	28.4	28.2	25.1
Or	26.1	26.0	24.4	24.3	22.0	21.7	20.0
Qtz	38.7	40.1	42.9	43.5	48.5	49.2	53.7
Cor	1.0	1.0	1.0	1.0	1.1	0.9	1.2
ASI	1.03 (0.04)	1.03 (0.02)	1.02 (0.02)	1.03 (0.03)	1.00 (0.03)	1.00 (0.04)	1.00 (0.04)

Imaging a combination of ^{9}Be and ^{23}Na allowed for crystal phases to be distinguished readily from each other and from glass pools. Additionally ^{27}Al, ^{39}K, and ^{30}Si were imaged for verification of glass pools suitable for analysis. Slight contamination by beryl, chrysoberyl, phenakite, or quartz in the sputtered volume greatly skewed the Be totals up or down, which further facilitated the selection of areas containing glass only.

DISCUSSION OF EXPERIMENTAL RESULTS

Anticipated phase relations

Compositions HGS4 and HGS5 are quartz-saturated only at their solidi and become increasingly silica-undersaturated with increasing temperature. The Phn mix (Phn + Cor + Qtz) is isochemical with beryl, and hence mixtures HGS4 + Brl, HGS4 + Phn mix, HGS5 + Brl, and HGS5 + Phn mix should all be quartz-undersaturated above their minima. Based on the phase relations of Figure 1, we could anticipate that stable assemblages for these compositions would include beryl + phenakite (HGS4 + Brl, HGS4 + Phn mix) and beryl + phenakite + chrysoberyl (HGS5 + Brl, and HGS5 + Phn mix). For this reason we created mixtures HGS4 + Brl + Qtz and HGS5 + Brl + Qtz to remain quartz-saturated at all temperatures above the solidus; from Figure 1, stable assemblages should be beryl + quartz and beryl + quartz + chrysoberyl, respectively. Tie lines in Figure 1 predict

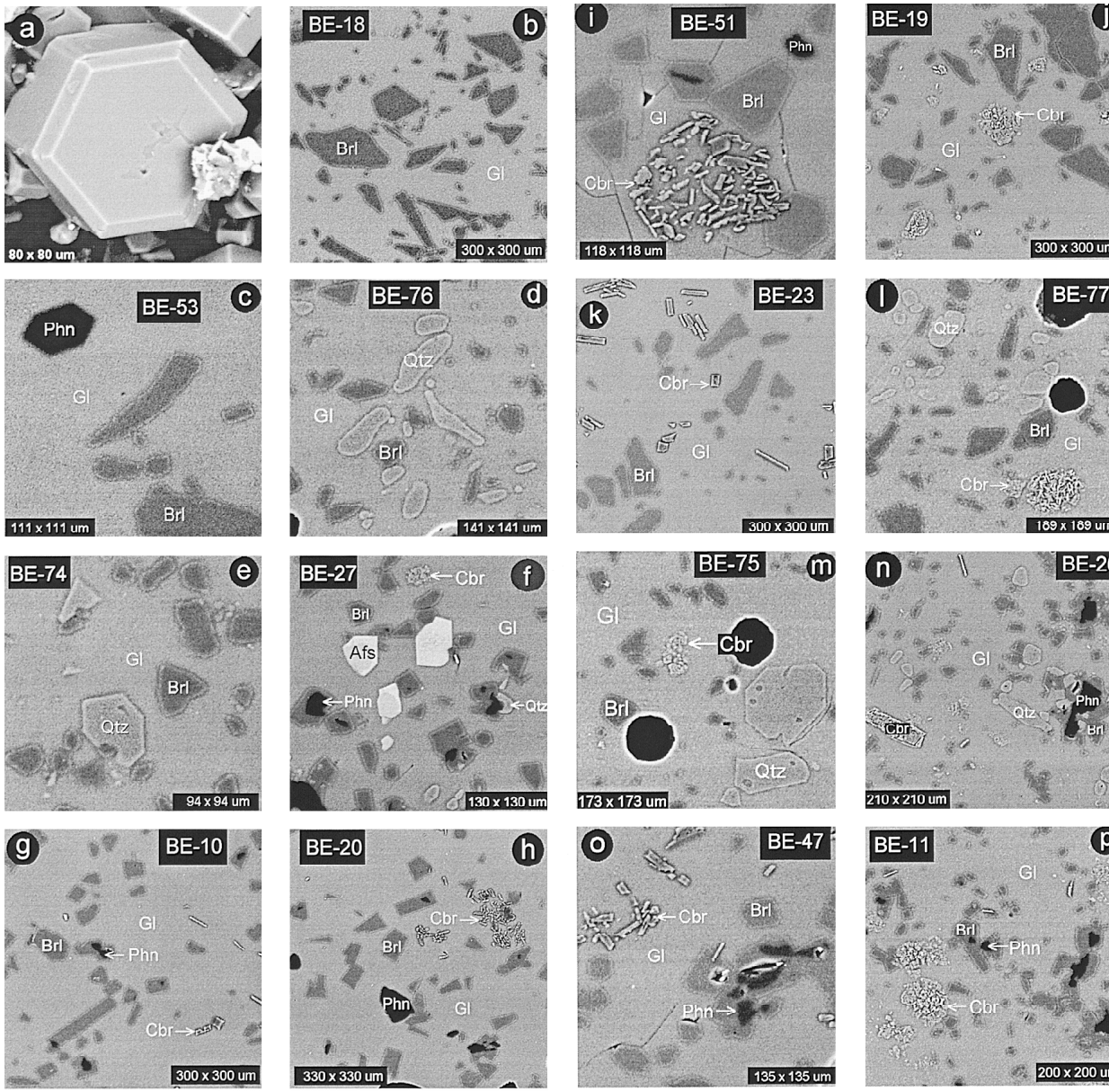

FIGURE 4. Secondary electron and backscattered electron micrographs of experimental products. **(a)** Subsolidus experiment with the mixture of phenakite + Al_2O_3 + quartz (Phn mix) demonstrating the successful derivation of beryl. **(b)** Relict beryl (Brl) and glass (Gl) from a forward-direction dissolution experiment at 750 °C using HGS4 + Brl. **(c)** Growth of new, euhedral beryl crystals in a reverse-direction experiment to 700 °C using HGS4. New phenakite (Phn) was stable with beryl and glass (Phn + Brl + melt). **(d)** Remnant anhedral quartz (Qtz) and beryl in glass confirmed Qtz saturation of melt in a forward-direction experiment at 850 °C using HGS4 + Brl + Qtz. **(e)** Reverse-direction experiment at 800 °C with HGS4 + Brl + Qtz showed new growth of both beryl and quartz. **(f)** Forward-direction experiment at 700 °C using HGS4 + Phn mix contained the assemblage alkali feldspar (Afs) + beryl + chrysoberyl (Cbr) + phenakite + quartz + glass, in which all phases were stable except phenakite (see text). Phenakite was completely armored by beryl; incorporation of Ba (from starting adularia) imparted bright BSE intensity to new growth of Afs. **(g)** Forward-direction experiment using HGS4 + Phn mix at 750 °C contained new beryl + new chrysoberyl + armored (beryl overgrowths on) phenakite + glass. **(h)** The reversal for the experiment in **(g)** contained new beryl + new chrysoberyl (in clusters) + unarmored phenakite + glass, indicating that the assemblage Brl + Cbr + Phn + melt was stable at these conditions. **(i)** A forward-direction experiment at 800 °C using HGS4 + Phn mix contained the same assemblage as **(g)** and **(h)** but coarser chrysoberyl. **(j)** Forward-direction experiment with HGS5 + Brl at 750 °C resulted in anhedral beryl + fine-grained clots of chrysoberyl + glass. **(k)** Reverse-direction experiment at 750 °C using HGS5 + Brl grew small euhedral beryl crystals + coarse, elongate chrysoberyl + glass. (l) Forward-direction experiment with HGS5 + Brl + Qtz 850 °C yielded anhedral and resorbed quartz + anhedral beryl + new chrysoberyl (in clots). **(m)** In the reverse-direction to 800 °C, HGS5 + Brl + Qtz formed new beryl + new quartz + fine-grained chrysoberyl aggregates. **(n)** Forward-direction experiment at 700 °C using HGS5 + Phn mix produced new beryl + new chrysoberyl + euhedral to subhedral quartz + phenakite in glass, but phenakite was completely

continued on next page

that beryl should not be stable with aluminosilicate or corundum for these experimental conditions, and that the most aluminous phase coexisting with beryl should be chrysoberyl. Among these two compositions, HGS5 + Brl + Qtz is closest to saturation in both silica and alumina.

Observed phase assemblages

HGS4 + Brl. The assemblage beryl + melt (Table 3a) was stable over the temperature interval investigated (700–850 °C) where forward-direction runs indicated beryl dissolution by resorption of anhedral crystals and reversals showed new beryl growth (Fig. 4b). In reversals, beryl formed new euhedral crystals (5–10 mm) but did not form distinct overgrowths on remnant beryl. Euhedral phenakite coexisted with beryl + melt (Fig. 4c) but only in reverse-direction experiments (BE-53 and BE-55, Table 3a) at 700 and 800 °C. Quartz was not present in any experimental results; hence, the stable assemblage, as expected, was beryl + phenakite + melt, although phenakite did not nucleate in forward-direction experiments.

HGS4 + Brl + Qtz. All run products (Table 3b) consisted of quartz + beryl + glass over the conditions investigated. Glasses contained anhedral and embayed quartz crystals in forward-direction experiments and coarse (~25 mm) euhedral quartz crystals, in some cases skeletal in structure, in reversals (Figs. 4d–e). Beryl dissolution was manifested by resorbed crystals; new growth was evident as small (5–10 mm), new crystals in reverse-direction experiments. The stable assemblage was beryl + quartz (along their tie line, Fig. 1) + glass.

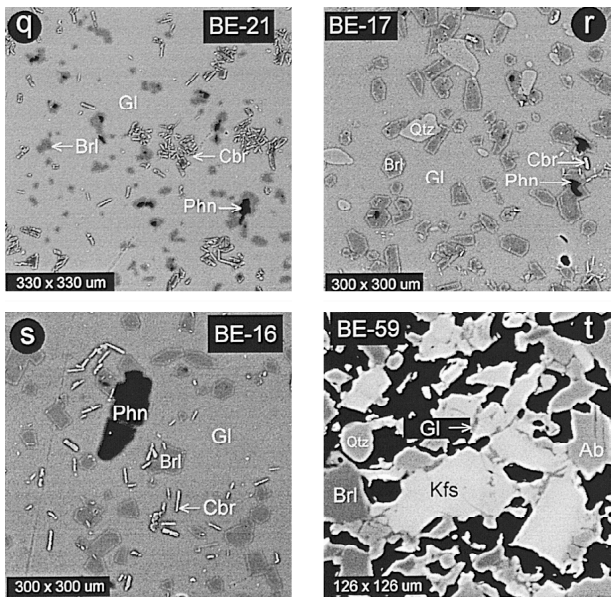

FIGURE 4.—*continued*
armored by beryl growth. **(o)** Growth experiment at 700 °C using the same composition as in (n) produced the assemblage of new beryl + new coarse-grained chrysoberyl + armored phenakite + glass. **(p)** A forward-direction experiment at 750 °C using HGS5 + Phn Mix contained the same assemblage as **(o)** but chrysoberyl occured as fine-grained clots. **(q)** The reversal for **(p)**, this experiment showed coarsening and dissemination of chrysoberyl clots. Phenakite was armored here but interpreted to be a stable phase (see text). **(r)** A forward-direction experiment at 650 °C using MAC + Phn Mix contained new beryl + new chrysoberyl + euhedral to subhedral quartz + phenakite with glass, but phenakite was again armored by beryl. **(s)** A forward-direction experiment at 850 °C with MAC + Phn mix contained unarmored phenakite with beryl, chrysoberyl and glass; quartz was absent. **(t)** Melting experiment at 680 °C using HGS4 + Brl (the composition most similar to haplogranite) contained minute glass pools between grains. This is the lowest temperature (in 5 °C increments) for which glass (melt) was observed.

HGS4 + Phn mix. The forward-direction experiment BE-27 at 700 °C (Table 3c) contained relict alkali feldspar and quartz + beryl + chrysoberyl + phenakite + melt (Fig. 4f). The reversal (BE-50, Table 3c), however, contained only phenakite + beryl + chrysoberyl with glass. New euhedral crystals of coarse-grained beryl (up to 90 mm) and fine acicular to coarse blocky chrysoberyl (~3–10 mm) occurred with relict phenakite in both forward-direction and reverse-direction experiments at 750 and 800 °C, and in the forward-direction 850 °C run (Table 3c, Figs. 4g–i). Rounded and resorbed phenakite crystals remained in contact with glass in all reverse-direction runs plus the 800 °C forward-direction experiment (BE-50, BE-20, BE-51, and BE-52, Table 3c). One possible interpretation of these results is that quartz persisted metastably in forward-direction experiment BE-27. In that near-solidus experiment, however, relic phenakite was rimmed completely by new beryl growth and, hence, isolated from the melt. We suggest that phenakite was removed from the reaction assemblage in this experiment before all quartz was consumed, and that the stable assemblage in BE-27 was actually beryl + chrysoberyl + quartz (Fig. 1). In the reverse-direction experiment BE-50 and all other experiments at higher temperature (Table 3c), phenakite remained in contact with melt and quartz was absent, indicating that the stable assemblage for the bulk composition HGS4 + Phn mix was indeed phenakite + beryl + chrysoberyl.

HGS5 + Brl. All forward-direction and reverse-direction experiments (Table 4a) contained relict beryl + chrysoberyl + melt. In forward-direction experiments, beryl was anhedral to subhedral and relict (slightly resorbed). Chrysoberyl formed fine-grained clots (~30 mm in diameter) in forward-direction runs and larger euhedral crystals (5–25 mm) in reversals (Figs. 4j–k). Similar to HGS4 + Brl, reversals contained no discernable overgrowths on preexisting beryl; new beryl occurred as small, euhedral (5–10 mm) crystals in glass. All experiments in this system produced approximately the same modal quantity of beryl as in HGS4 systems, but modal chrysoberyl was approximately double that of the HGS4 + Phn experiments. From Figure 1, these experiments should have contained some phenakite, but none nucleated in either forward- or reverse-directions.

HGS5 + Brl + Qtz. The products for this composition were beryl + quartz + chrysoberyl (all runs, Table 4b, Figs. 4l–m), which is consistent with the topology of Figure 1. Modal chrysoberyl was significantly lower in these products compared to other HGS5 compositions.

HGS5 + Phn mix. The forward-direction run at 700 °C (BE-26, Table 4c) contained relict quartz and phenakite + beryl + chrysoberyl + melt (Fig. 4n). Quartz was not present in the 700 °C reversal (BE-47, Table 4c, Fig. 4o) or in experiments at higher temperatures (Figs. 4p–q). Similar observations in HGS4 + Phn mix lead us to the same conclusions: The stable assemblage for the

TABLE 3c. Glass compositions of HGS4 run products—HGS4 + Phn Mix experiments

Run no.	BE-27	BE-50	BE-10	BE-20	BE-51	BE-52	BE-9
Temp. (°C)–Path	700-F	700-R	750-F	750-R	800-F	800-R	850-F
t (h) at T_{final}	960	720	700	816	600	672	144
Mineral products	Brl, Cbr, Afs, Qtz, (Phn)	Brl, Cbr, Phn	Brl, Cbr, Phn	Brl, Cbr, Phn	Brl, Cbr, Phn	Brl, Cbr, Phn	Brl, Cbr, Phn
No. of analyses	5	12	5	5	12	12	16
				weight percentage			
SiO_2	72.96 (0.66)	72.69 (0.54)	72.58 (0.42)	73.85 (0.25)	73.07 (0.45)	72.32 (0.62)	74.82 (0.42)
TiO_2	0.01 (0.01)	0.01 (0.01)	0.01 (0.01)	0.01 (0.01)	0.01 (0.01)	0.01 (0.01)	nd
Al_2O_3	12.45 (0.28)	11.57 (0.26)	11.84 (0.22)	11.89 (0.17)	12.21 (0.24)	12.06 (0.21)	11.52 (0.22)
FeO	0.01 (0.00)	0.01 (0.01)	0.01 (0.01)	0.01 (0.01)	0.02 (0.01)	0.01 (0.01)	nd
MnO	0.01 (0.01)	0.00 (0.00)	0.00 (0.00)	0.01 (0.01)	0.01 (0.01)	0.01 (0.01)	nd
BeO (ppm)	468 (5)	681 (2)	833 (10)	831 (10)	1428 (3)	1425 (3)	1887 (21)
MgO	0.00 (0.00)	0.00 (0.00)	0.00 (0.00)	0.00 (0.00)	0.00 (0.00)	0.00 (0.00)	nd
CaO	0.03 (0.01)	0.05 (0.02)	0.02 (0.02)	0.04 (0.03)	0.04 (0.02)	0.04 (0.02)	0.02 (0.02)
BaO	0.05 (0.05)	0.10 (0.04)	0.13 (0.04)	0.06 (0.02)	0.10 (0.04)	0.12 (0.04)	nd
Na_2O	3.89 (0.16)	3.63 (0.13)	3.86 (0.10)	3.88 (0.12)	3.80 (0.13)	3.77 (0.07)	3.52 (0.14)
K_2O	4.18 (0.07)	3.82 (0.12)	4.13 (0.05)	4.09 (0.06)	3.99 (0.17)	3.83 (0.12)	3.83 (0.07)
P_2O_5	0.18 (0.05)	0.03 (0.02)	0.21 (0.05)	0.18 (0.06)	0.03 (0.02)	0.02 (0.02)	nd
F	0.05 (0.05)	0.04 (0.04)	0.05 (0.05)	0.06 (0.06)	0.04 (0.04)	0.02 (0.01)	nd
F = O	–0.02 (0.02)	–0.02 (0.02)	–0.02 (0.02)	–0.03 (0.03)	–0.02 (0.02)	–0.01 (0.00)	nd
Total	93.85	92.00	92.90	94.13	93.44	92.34	93.90
H_2O diff	6.15	8.00	7.10	5.87	6.56	7.66	6.10
				CIPW normative %			
Ab	35.2	33.5	35.4	35.0	34.5	34.7	31.8
Or	26.4	24.6	26.4	25.8	25.3	24.6	24.2
Qtz	36.7	40.3	37.2	38.0	38.4	38.8	42.4
Cor	1.6	1.6	1.1	1.2	1.8	1.9	1.7
ASI	1.11 (0.03)	1.10 (0.04)	1.05 (0.02)	1.06 (0.02)	1.09 (0.02)	1.10 (0.02)	1.07 (0.03)

TABLE 4a. Glass compositions of HGS5 run products—HGS5 + Brl experiments

Run no.	BE-78	BE-19	BE-23	BE-13
Temp. (°C)–Path	700-R	750-F	750-R	850-F
t (h) at T_{final}	700	980	816	144
Mineral products	Brl, Cbr	Brl, Cbr	Brl, Cbr	Brl, Cbr
No. of analyses	12	5	5	13
		weight percent		
SiO_2	71.72 (0.37)	72.41 (0.32)	73.64 (0.32)	72.21 (0.32)
TiO_2	nd	0.01 (0.01)	0.01 (0.01)	nd
Al_2O_3	13.02 (0.12)	12.87 (0.12)	12.36 (0.20)	13.22 (0.11)
FeO	nd	0.02 (0.01)	0.04 (0.01)	nd
MnO	nd	0.00 (0.00)	0.00 (0.00)	nd
BeO (ppm)	349 (1)	582 (6)	571 (6)	1314 (15)
MgO	nd	0.00 (0.00)	0.01 (0.00)	nd
CaO	0.02 (0.02)	0.04 (0.03)	0.01 (0.01)	0.02 (0.02)
BaO	nd	0.10 (0.02)	0.07 (0.06)	nd
Na_2O	3.66 (0.12)	3.84 (0.15)	3.79 (0.06)	3.92 (0.11)
K_2O	4.10 (0.10)	3.92 (0.11)	3.76 (0.19)	3.81 (0.14)
P_2O_5	nd	0.16 (0.05)	0.18 (0.04)	nd
F	nd	0.11 (0.11)	0.13 (0.13)	nd
F = O	nd	–0.05 (0.05)	–0.05 (0.05)	nd
Total	92.55	93.49	94.01	93.31
H_2O diff	7.45	6.51	5.99	6.69
		CIPW normative %		
Ab	33.4	34.9	34.3	35.6
Or	26.2	24.9	23.7	24.2
Qtz	37.6	37.7	39.8	37.4
Cor	2.8	2.5	2.2	2.8
ASI	1.22 (0.04)	1.18 (0.02)	1.16 (0.02)	1.19 (0.04)

bulk composition HGS5 + Phn mix is phenakite + beryl + chrysoberyl. Because phenakite became armored completely by new beryl in the forward-direction experiment at 700 °C, the resultant reactive assemblage was no longer Phn-saturated and moved off the composition of Brl (= Phn + Cor + Qtz in the Phn mixes) into the divariant space of Chr + Brl + Qtz (Fig. 1).

Between 750–850 °C the assemblage beryl + chrysoberyl + phenakite + melt is stable, but the textural differences (Figs. 4p–q) of chrysoberyl between forward-direction and reverse-direction pathways are distinctive. Chrysoberyl formed fine-grained clots (~40 mm in diameter) in forward-direction experiments and coarse, euhedral crystals (5–20 μm), which occurred in clusters (former clots) in reverse-direction experiments. In all experiments (Table 4c), beryl formed coarse (~25 mm) euhedral crystals and phenakite was rounded and extensively armored by beryl. Modal chrysoberyl was greater than that of HGS5 + Brl, but no significant change was observed in the proportions of the other crystalline components.

MAC systems. MAC + Brl compositions (Table 5) contained beryl + chrysoberyl + glass over the temperature range 650–850

TABLE 4b. Glass compositions of HGS5 run products—HGS5 + Brl + Qtz experiments

Run no.	BE-65	BE-67	BE-69	BE-71	BE-73	BE-75	BE-77
Temp. (°C)–Path	700-F	700-R	750-F	750-R	800-F	800-R	850-F
t (h) at T_{final}	720	700	720	792	408	408	168
Mineral products	Brl, Cbr, Qtz	Brl, Cbr, Qtz	Brl, Cbr, Qtz	Brl, Cbr, Qtz	Brl, Cbr, Qtz	Brl, Cbr, Qtz	Brl, Cbr, Qtz
No. of analyses	12	12	12	12	11	12	12
				weight percent			
SiO_2	73.01 (0.54)	73.61 (0.36)	74.02 (0.62)	74.73 (0.43)	76.00 (0.57)	75.86 (0.42)	76.86 (0.84)
Al_2O_3	12.60 (0.33)	12.02 (0.18)	11.90 (0.30)	11.69 (0.18)	11.09 (0.08)	10.81 (0.10)	10.22 (0.17)
BeO (ppm)	406 (23)	289 (24)	556 (24)	452 (13)	812 (19)	982 (6)	1188 (10)
CaO	0.02 (0.02)	0.03 (0.02)	0.03 (0.02)	0.03 (0.01)	0.02 (0.01)	0.02 (0.02)	0.03 (0.02)
Na_2O	3.36 (0.08)	3.29 (0.12)	3.16 (0.08)	3.16 (0.12)	2.83 (0.09)	2.78 (0.07)	2.52 (0.09)
K_2O	3.82 (0.09)	3.75 (0.11)	3.58 (0.13)	3.56 (0.12)	3.20 (0.07)	3.11 (0.08)	2.84 (0.06)
Total	92.85	92.73	92.75	93.22	93.22	92.68	92.59
H_2O diff	7.15	7.27	7.25	6.78	6.78	7.32	7.41
				CIPW normative %			
Ab	30.6	30.0	28.9	28.7	25.7	25.4	23.1
Or	24.3	23.9	22.8	22.6	20.3	19.9	18.2
Qtz	41.9	43.3	45.3	45.9	50.8	51.6	55.5
Cor	3.2	2.8	3.1	2.8	3.2	3.1	3.3
ASI	1.28 (0.04)	1.24 (0.03)	1.27 (0.04)	1.25 (0.03)	1.31 (0.03)	1.29 (0.02)	1.32 (0.04)

TABLE 4c. Glass compositions of HGS5 run products—HGS5 + Phn Mix experiments

Run no.	BE-26	BE-47	BE-11	BE-21	BE-49	BE-12
Temp. (°C)–Path	700-F	700-R	750-F	750-R	800-R	850-F
t (h) at T_{final}	960	744	700	816	576	144
Mineral products	Brl, Cbr, Qtz, (Phn)	Brl, Cbr, Phn	Brl, Cbr, Phn	Brl, Cbr, Phn	Brl, Cbr, Phn	Brl, Cbr, Phn
No. of analyses	5	12	5	6	12	15
			weight percentage			
SiO_2	72.97 (0.29)	73.94 (0.56)	72.53 (0.84)	74.39 (0.33)	74.07 (0.60)	73.77 (0.58)
TiO_2	0.01 (0.01)	0.01 (0.01)	0.00 (0.00)	0.01 (0.01)	0.01 (0.01)	nd
Al_2O_3	12.51 (0.10)	11.94 (0.30)	12.03 (0.18)	11.67 (0.17)	11.98 (0.26)	12.22 (0.36)
FeO	0.00 (0.00)	0.01 (0.01)	0.02 (0.01)	0.01 (0.01)	0.01 (0.01)	nd
MnO	0.00 (0.00)	0.01 (0.01)	0.00 (0.00)	0.00 (0.00)	0.00 (0.00)	nd
BeO (ppm)	327 (4)	341 (1)	586 (6)	585 (6)	971 (1)	1337 (15)
MgO	0.00 (0.00)	0.00 (0.00)	0.00 (0.00)	0.00 (0.00)	0.00 (0.00)	nd
CaO	0.04 (0.02)	0.03 (0.02)	0.03 (0.02)	0.03 (0.02)	0.02 (0.02)	0.02 (0.02)
BaO	0.08 (0.05)	0.08 (0.04)	0.08 (0.05)	0.08 (0.04)	0.08 (0.04)	nd
Na_2O	3.67 (0.15)	3.58 (0.12)	3.73 (0.10)	3.77 (0.08)	3.57 (0.15)	3.58 (0.16)
K_2O	3.73 (0.12)	3.51 (0.09)	3.63 (0.11)	3.62 (0.08)	3.43 (0.10)	3.63 (0.08)
P_2O_5	0.17 (0.03)	0.02 (0.02)	0.17 (0.03)	0.19 (0.06)	0.02 (0.02)	nd
F	0.08 (0.08)	0.04 (0.03)	0.06 (0.06)	0.10 (0.10)	0.04 (0.03)	nd
F = O	–0.03 (0.03)	–0.01 (0.01)	–0.02 (0.02)	–0.04 (0.04)	–0.02 (0.01)	nd
Total	93.26	93.19	92.32	93.89	93.31	93.35
H_2O diff	6.74	6.81	7.68	6.11	6.69	6.65
			CIPW normative %			
Ab	33.4	32.6	34.3	34.1	32.4	32.5
Or	23.7	22.3	23.3	22.9	22.3	23.0
Qtz	40.2	42.7	40.2	41.3	42.8	41.9
Cor	2.6	2.4	2.1	1.7	2.5	2.6
ASI	1.21 (0.03)	1.21 (0.05)	1.16 (0.03)	1.12 (0.01)	1.19 (0.06)	1.18 (0.05)

°C; forward-direction experiments for MAC + Phn mix runs (Table 5) yielded beryl + chrysoberyl + phenakite + glass over the same interval. As with the other Phn mix compositions (HGS4 and HGS5), phenakite was armored completely by beryl in only one run with MAC + Phn Mix: the BE-17 forward-direction experiment at 650 °C (Table 5, Fig. 4r). Using the previous criteria, we believe that the stable assemblage is beryl + chrysoberyl + phenakite + glass, despite the observed product assemblage Brl + Cbr + Qtz + glass, owing to isolation of phenakite by Brl overgrowths. Otherwise, the assemblages for both systems (Brl and Phn mix) were quartz-absent and identical in forward-direction and reverse-direction pathways (Table 5). Phenakite occurred as unarmored anhedral grains or armored by new beryl (Fig. 4s). Coarse, anhedral (heavily resorbed) beryl persisted in forward-direction runs of MAC + Brl, and small (5–10 μm) euhedral crystals were found in the reversals. Beryl grown from the MAC + Phn mix was coarse-grained and euhedral. Chrysoberyl formed isolated euhedral crystals in all cases, whereas chrysoberyl clots (coarse or fine-grained) were notably absent from these run products. The likely stable assemblage above the solidus is phenakite + beryl + chrysoberyl (+ melt), although phenakite was absent in the MAC + Brl experiments.

BeO contents of melt at beryl saturation

For each bulk composition, the BeO contents of glasses in beryl-saturated experiments increased from 700 to 850 °C. All

Table 5. Glass compositions of MAC run products

	MAC + Brl experiments			MAC + Phn Mix experiments			
Run no.	BE-24	BE-31	BEJ-27*	BE-17	BE-30	BEJ-30	BE-16
Temp. (°C)–Path	650-F	650-R	750-F	650-F	650-R	750-F	850-F
t (h) at T_{final}	980	936	624	980	936	624	144
Minerals‡	Brl, Cbr, Zrc	Brl, Cbr	Brl, Cbr	Brl, Cbr, Qtz, (Phn)	Brl, Cbr, Phn	Brl, Cbr, Phn	Brl, Cbr, Phn
No. of analyses	6	5		5	5	5	5
				weight percent			
SiO_2	66.88 (0.58)	67.66 (0.52)	65.81 (0.35)	67.77 (0.53)	68.27 (0.49)	66.21 (0.48)	68.17 (0.54)
TiO_2	0.03 (0.02)	0.03 (0.01)	0.02 (0.00)	0.02 (0.01)	0.02 (0.01)	0.02 (0.02)	0.03 (0.01)
Al_2O_3	14.68 (0.09)	14.31 (0.20)	13.28 (0.24)	13.47 (0.09)	13.78 (0.11)	13.46 (0.18)	12.78 (0.23)
FeO	0.50 (0.02)	0.04 (0.00)	0.49 (0.03)	0.23 (0.01)	0.01 (0.01)	0.28 (0.01)	0.36 (0.02)
MnO	0.05 (0.01)	0.06 (0.01)	0.05 (0.01)	0.05 (0.02)	0.05 (0.01)	0.03 (0.02)	0.05 (0.01)
BeO (ppm)	598 (7)	588 (7)	1240 (21)	596 (7)	622 (7)	1030 (14)	4016 (44)
MgO	0.01 (0.01)	0.01 (0.00)	0.00	0.00 (0.00)	0.00 (0.00)	0.01 (0.01)	0.01 (0.00)
CaO	0.22 (0.04)	0.20 (0.03)	0.21 (0.01)	0.18 (0.02)	0.20 (0.03)	0.20 (0.02)	0.18 (0.02)
BaO	0.04 (0.02)	0.02 (0.02)	0.01 (0.00)	0.01 (0.01)	0.01 (0.01)	0.02 (0.01)	0.02 (0.02)
Na_2O	3.46 (0.17)	3.54 (0.09)	3.30 (0.17)	3.44 (0.08)	3.56 (0.12)	3.35 (0.26)	3.31 (0.05)
K_2O	3.37 (0.09)	3.43 (0.13)	3.20 (0.12)	3.34 (0.06)	3.44 (0.15)	3.30 (0.14)	3.14 (0.05)
P_2O_5	0.66 (0.04)	0.75 (0.05)	nd	0.62 (0.06)	0.74 (0.07)	nd	0.64 (0.05)
F	1.39 (0.24)	1.36 (0.17)	nd	1.29 (0.07)	1.37 (0.16)	nd	1.24 (0.09)
O = F	–0.59 (0.10)	–0.57 (0.07)	–0.54 (0.03)	–0.58 (0.07)	–0.52 (0.04)		
Total	90.76	90.90	86.49	89.94	90.93	86.88	89.81
H_2O diff	9.24	9.10	13.51	10.06	9.07	13.12	10.19
				CIPW normative %			
Ab	33.1	33.7	31.8	33.1	33.8	32.8	32.0
Or	22.5	22.8	22.7	22.4	22.8	22.6	21.2
Qtz	38.3	38.1	40.3	39.7	38.6	39.5	42.2
Cor	6.0	5.4	5.2	4.8	4.7	5.1	4.5
ASI†	1.31 (0.06)	1.26 (0.02)	1.26 (0.02)	1.22 (0.03)	1.21 (0.05)	1.24 (0.02)	1.06 (0.01)

* BEJ- identifies experiments performed at CSM; experiments reported with BE- notation are from OU.
† Zrc = zircon.
‡ ASI values account for Li_2O (not shown here).

glass products analysed in this study contained less—in some cases far less—than 0.5 wt% BeO (≈3 normative wt% beryl). Beryllia contents of melt varied linearly between 750 to 850 °C (Fig. 5) but the BeO concentrations leveled off between 700 to 750 °C for all compositions studied. We interpret the deviation from linearity at lower temperatures to reflect increasingly steep curvature of the beryl liquidus surface near the minimum of the system (as is observed for the liquidus surface of the feldspars: Tuttle and Bowen 1958).

The dissolution or precipitation of beryl from melt can be related to the activity relationship:

$$(a_{Be_3Al_2Si_6O_{18}})_{beryl} = (a_{BeO})^3_{melt}(a\mathrm{Al_2O_3})(a\mathrm{SiO_2})^6 \quad (3)$$

in which the activity of a beryl component in melt is a function of the activities of its constituent oxides. This representation emphasizes the importance of silica activity and, to a lesser extent, alumina activity (monitored through the parameter of ASI) on the BeO content of melt at beryl saturation, and it allows us to consider the effects of other components (e.g., B, P, or F) on the activities of the individual beryl-forming components.

Effect of silica activity. The activity of the beryl component in melt varies as the sixth power of silica activity; consequently, variations in the activity of SiO_2 will effect major changes in the BeO content of melt at beryl saturation. We see this in the data for HGS4 + Brl with and without quartz saturation. Both compositions were quartz-saturated at their solidi, but HGS4 + Brl became increasingly silica-undersaturated with increasing temperature. The BeO contents of melts from HGS4 + Brl ranged from 1118 ppm BeO at 700 °C to 3136 ppm BeO at 850 °C (Table 3a, Fig. 5). The BeO content of melts derived from HGS4 + Brl + Qtz, in which quartz saturation was maintained at all temperatures, was similar at 700 °C (mean 1264 ppm) but was only 2569 ppm BeO at 850 °C—lower at high temperature because of the higher activity of silica in the quartz-saturated experiments. As beryl-bearing pegmatites are typically quartz-saturated, the solubility data for HGS4 + Brl + Qtz are more relevant.

Effect of alumina activity. The solubility of beryl in melt varies as the first power of the activity of alumina in melt. In this system, the alumina-saturating phase in equilibrium with beryl was chrysoberyl, which corroborates previous interpretations of the chemography (Burt 1978; Barton 1986) shown in Figure 1. At the high ASI of the chrysoberyl-saturated runs using HGS5, the BeO contents of melts were displaced systematically (parallel to HGS4 results) to lower values. Beryllia contents for HGS5 + Brl increased from 349 to 1314 ppm BeO from 700 to 850 °C. As expected, experiments that were saturated in both quartz and chrysoberyl (HGS5 + Brl + Qtz) displayed the lowest BeO contents in melt at any temperature. For this system, BeO values increased from 289 to 1188 ppm over the same temperature interval. Experiments with HGS4 + Phn mix produced melts whose ASI values were intermediate between HGS4 + Brl and all HGS5 experiments. The BeO contents of glasses for HGS4 + Phn mix were intermediate as well (Fig. 5). There was little discernible difference in the BeO concentrations in glasses derived from HGS5 + Phn mix vs. HGS5 + Brl + Qtz: both compositions are strongly peraluminous and near saturation in silica.

Effects of other components. The Macusani glass is high

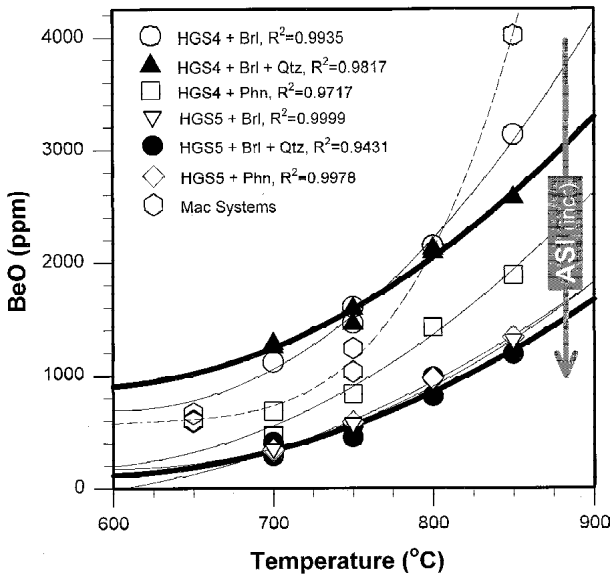

FIGURE 5. BeO contents of experimental products from 650–850 °C and 200 MPa (H_2O). The thick curves are for quartz-saturated experiments. The vertical arrow represents increasing melt ASI from 1.00 to 1.28 among HGS4 and HGS5 systems. The experimental trend using macusanite (ASI = 1.22) lies in the opposite direction of increasing ASI. Analytical and instrumental error are less than symbol sizes.

in silica and strongly peraluminous with an ASI = 1.31 (including Li in the total of alkalis). In contrast to the experiments with HGS5 ± Qtz, however, results of MAC + Brl or Phn mix were very similar and yielded the highest BeO contents of any experiments: For MAC + Phn mix, BeO values of glass ranged from 588 to 4016 ppm between 700 to 850 °C. Overall, the solubility data (Fig. 5) fit an exponential trend (to a second-order polynomial) better than a linear trend, but the curvature is similar to that of the other systems. The disparity between MAC and the HGS5 results might have resulted from speciation reactions among Be or Al and the more numerous components of the Macusani glass (Li, B, P, F, Rb, and Cs—all at 10^4–10^5 ppm levels). The components of F and P are known to associate structurally with Al in glasses (e.g., Manning et al. 1980; Mysen and Virgo 1985; Gan and Hess 1989). The local environment of B in hydrous granitic glass is not known with sufficient certainty to determine the effect of B on the $a_{Al_2O_3}$ in melt (Morgan et al. 1990), but alkaline B solutions do increase the solubility of Al in aqueous fluid substantially (Morgan and London 1989). These components, therefore, might be expected to reduce the activity of Al_2O_3 in macusanite liquid. Despite the increased solubility of beryl in the macusanite melts, however, these experiments remained saturated in chrysoberyl. Thus, for this composition, speciation among Be and the other components might have been the more important factor (e.g., Be-F complexation; Toth et al. 1973).

Figure 5 illustrates that BeO contents increase between peraluminous granitic compositions in the order: HGS5 + Brl + Qtz < HGS5 + Brl ≈ HGS5 + Phn Mix < HGS4 + Phn mix < HGS4 + Brl + Qtz < HGS4 + Brl < MAC, which, with the exception of macusanite, reflects a decreasing trend in melt ASI. However, despite differences between BeO in macusanite and BeO contents of haplogranites at 850 °C, note that all BeO values tend to converge at low temperatures.

Effects of beryllium on the liquidus phase relations

After subtracting the normative beryl components of the glasses (based on the SIMS analyses of BeO), the normative Ab, Or, and Qtz components of glasses derived from HGS4 + Brl were compared to those of HGS4 only. Table 6 shows an internally consistent shift of the minimum melt composition toward the SiO_2 melt component; however, the magnitude of the shift, 4.5 normative wt% Qtz, is small. Equally minor in magnitude, but measurable, is a decrease in the solidus of the system by ~10 °C with the addition of Be (Table 7, Fig. 4t), from 690–685 °C (HGS4) to 680–675 °C (HGS4 + Brl).

Structural environment of Be in melt. Compared to other crystalline alkali or alkaline earth aluminosilicates, the solubility of beryl in granitic melts is low (<0.5 wt% BeO, or much lower). This result begs the question of why Be should behave differently from the other cations, which tend to have coordination numbers in minerals ≥6 and act as network-modifying components of the melt structure. Because of its small size (ionic radius of $^{IV}Be^{2+}$ = 0.27 Å: Shannon 1976) and the appreciable covalency of its bonds, Be invariably occurs in tetrahedral coordination in crystalline silicates (e.g., Pauling 1960; Wuensch and Hörmann 1978) and in the silicate glasses stud-

TABLE 6. Near-solidus glass compositions or Be-bearing and Be-absent HGS4

	Near-solidus glass compositions	
Powder	HGS4	HGS4 + Brl
Run no.	HGS4-1	BE-79
Temp. (°C)–Path	700-F	700-F
t (h) at T_{final}	720	744
Mineral products	Ab, Or, Qtz	Ab, Or, Qtz, Brl
No. of analyses	20	12
	weight percent	
SiO_2	72.32 (0.25)	72.16* (0.75)
TiO_2	nd	0.01 (0.01)
Al_2O_3	11.65 (0.39)	11.39* (0.06)
FeO	nd	0.06 (0.01)
MnO	nd	0.01 (0.01)
MgO	nd	0.00
CaO	0.02 (0.02)	0.05 (0.02)
BaO	nd	0.06 (0.04)
Na_2O	4.14 (0.20)	4.00 (0.10)
K_2O	4.50 (0.14)	3.77 (0.14)
P_2O_5	nd	0.03 (0.02)
F	nd	0.02 (0.03)
F = O	nd	-0.01
Total	92.63	92.17†
H_2O diff	7.37	7.83
	CIPW normative %	
Ab	37.8	37.4
Or	28.7	24.6
Qtz	33.5	38.0
ASI	1.00 (0.04)	1.03 (0.02)

* SiO_2 and Al_2O_3 contents are adjusted by subtracting their normalized beryl components (estimated BeO content = 1000 ppm; see Table 2, Fig. 5) in order to represent melt composition as a function of Be addition (not beryl addition). The adjustment resulted in less ~0.7% of both silica and alumina totals, but the analysis total (†) reflects original (real) values.

TABLE 7. Melting experiments for Be-bearing and Be-absent HGS4

			HGS4 melting runs			
Run no.			BE-63	BE-60	BE-61	BE-62
Temp. (°C)–Path			680-F	685-F	690-F	695-F
t (h)			864	864	864	864
Run products			Ab, Or, Qtz	Ab, Or, Qtz	Ab, Or, Qtz, glass	Ab, Or, Qtz, glass
			HGS4 + Brl melting runs			
Run no.	BE-87	BE-81	BE-59	BE-58	BE-57	BE-56
Temp. (°C)–Path	670-F	675-F	680-F	685-F	690-F	695-F
t (h)	744	744	864	864	864	864
Run products	Ab, Or, Qtz, Brl	Ab, Or, Qtz, Brl	Ab, Or, Qtz, Brl, glass	Ab, Or, Qtz, Brl, glass	Ab, Or, Qtz, Brl, glass	Ab, Or, Qtz, Brl, glass

ied to date (Riebling and Duke 1967). Its field strength (Z/r^2 = 27.43) is intermediate between but nearer to that of Al (19.72) than to Si (59.17).

In this study, BeO was included in the denominator of the ASI calculation on the assumption that metaluminous melts, e.g., HGS4, remained fully polymerized after the addition of beryl components. This treatment, in which Be is regarded as a charge-balancing cation for ^{VI}Al, is clearly inaccurate for several reasons. The first is that Be does not possess the normal coordination number and field strength of the typical network-modifying cations. Based on viscosity measurements of haplogranitic liquids, BeO does not act as a network-modifier in the same way as the alkalis or other alkaline earths (Hess et al. 1995; Dingwell et al. 1996). In addition, with the congruent dissolution of beryl into melt, the sum of charge from 3 Be^{2+} + 2 Al^{3+} is > 2 Si^{4+}. In other words, beryl can be thought of as contributing 1 $BeAl_2O_4$ + 2 BeO to melt. All features considered, Be would appear to proxy better for Al than for Si in melt, and we might have included Be in the numerator of the ASI. In lieu of any further knowledge of the structural environment and role of Be in granitic melts, however, we have left Be in the denominator of the ASI, which has the approximate effect of removing the Be and Al components of beryl from the ASI calculation completely.

Beryl saturation in granitic pegmatite magmas

Distinctly beryl-rich granitic pegmatites are affiliated with the LCT family (for Li-Cs-Ta: Černý 1991a). According to Černý (1991b), the pegmatites of this family are leucocratic, potassic, and peraluminous. They are derived from mostly S- or mixed S- plus I-type granites, which in turn originated from supracrustal gneisses and schists that were undepleted by prior melting events. Within these sources, the micas and (at shallow pressures) cordierite are the likely resevoirs of most Be (Armbruster and Irouschek 1983; Griffits and Cooley 1961; Wuensch and Hörmann 1979), and contributions from these minerals during anatexis provide an initial enrichment of Be in melt. On average, however, granites contain only ~4–8 ppm Be (Beus 1966; Norton and Redden 1990). In view of the experiments reported here, such low Be values explain why beryl is not a magmatic phase in most granites. The beryl-bearing pegmatites derived from such granites presumably contained higher quantities of BeO, but the question remains how much?

In this study, we have identified three factors that will influence the precipitation of beryl in pegmatites: temperature, the activity of alumina (and silica), and the addition of other fluxing components. The lowest BeO contents needed to saturate melt in beryl are found in the experiments that are peraluminous and quartz-saturated but otherwise simple in composition. These correspond very closely to the beryl-type pegmatites of the LCT family (Černý 1991a), which are typically found not far beyond the margins of a parental granite (where exposed). More evolved LCT pegmatites of the complex-type remain beryl-saturated but tend to lie further from the parental granite source. The experiments reported here with the Macusani glass indicate that these magmas should require comparatively higher BeO contents to achieve beryl saturation. However, the complex-type pegmatites also lie in rocks of lower metamorphic grade (Černý 1991b) that were logically cooler than those that host the beryl-type pegmatites closer to the source. Fluxing components in the complex LCT pegmatites also lower the temperatures of their crystallization (e.g., London 1996). Thus, lower temperatures of crystallization may offset higher BeO contents required to saturate these flux-rich melts in beryl.

Our experimental results indicate that the BeO contents of all granitic melts studied at beryl saturation fall sharply with temperature, although more gradually as magmas approach their solidi, to converge at a range of similarly low BeO contents at low temperatures. Supercooling (e.g., below ~600–650 °C) of magmas represents the most effective means to bring pegmatite melts containing a few hundred ppm BeO to beryl saturation. The few available case histories of cooling rates in complex pegmatite dikes (Chakoumakos and Lumpkin 1990; Webber et al. 1997; Morgan and London, in review) all indicate that these magmas would have cooled below their solidi quickly (in days to months), and it is unlikely that crystallization would have kept pace with cooling (London 1996). At temperatures of ~450–550 °C, granitic pegmatites would become saturated in beryl at only a few tens to hundreds of parts per million of BeO in melt, depending upon the activity of alumina in the melts. Thus, we conclude that although beryl-rich pegmatites probably contained in their bulk magmas more Be than did their source granites, the enrichment need not have been more than ~5–10 times the granite average.

ACKNOWLEDGMENTS

Financial support for this research was provided by NSF grant EAR-9618867 to D. London and EAR-9316197 to R. Wendlandt, as well as a grant from CSM and from the Society of Economic Geologists Foundation. It is a pleasure to thank George Morgan and Greg Meeker for assistance with the electron probe data, Wendy Harrison for help with the ICP acquisitions, Michael Wiedenbeck for assistance with the SIMS data, and Gene Foord for donating a synthetic emerald from his personal supply for analytical calibration of Be. Mark Barton, PetrČerný, and Don Dingwell provided thoughtful reviews that improved the manuscript.

REFERENCES CITED

Armbruster, T. and Irouschek, A. (1983) Cordierites from the Lepontine Alps: Na + Be → Al substitution, gas content, cell parameters, and optics. Contributions to Mineralogy and Petrology, 82, 389–396.

Armstrong, J.T. (1989) CITZAF: Combined ZAF and phi-rho (Z) electron beam correction programs. California Institute of Technology, Pasadena, California.

Barnes, V.E., Edwards, G., McLaughlin, W.A., Friedman, I., and Joensuu, O. (1970) Macusanite occurrence, age and composition, Macusani, Peru. Geological Society of America Bulletin, 81, 1539–1546.

Barton, M.D. (1986) Phase equilibria and thermodynamic properties of minerals in the BeO-Al_2O_3-SiO_2-H_2O (BASH) system, with petrologic applications. American Mineralogist, 71, 277–300.

Beus, A.A. (1966) Geochemistry of Beryllium and Genetic Types of Beryllium Deposits, 286 p. Freeman, San Francisco.

Burt, D.M. (1978) Multisystems analysis of beryllium mineral stabilities: the system BeO-Al_2O_3-SiO_2-H_2O. American Mineralogist, 63, 664–676.

Cemic, L., Langer, K., and Franz, G. (1986) Experimental determination of melting relationships of beryl in the system BeO-Al_2O_3-SiO_2-H_2O between 10 and 25 kbar. Mineralogical Magazine, 50, 55–61.

Černý, P. (1991a) Rare-element granite pegmatites. Part I: anatomy and internal evolution of pegmatite deposits. Geoscience Canada, 18, 49–67.

——— (1991b) Rare-element granite pegmatites. Part II: regional to global environments and petrogenesis. Geoscience Canada, 18, 68–81.

Crock, J.G., Liche, F.E., and Briggs, P.H. (1983) Determination of the elements in the National Bureau of Standards geologic references materials SRM 278 obsidian and SRM 688 basalt by inductively-coupled argon plasma-atomic emission spectroscopy. Geostandards Newsletter, 7, 335–340.

Chakoumakos, B.C. and Lumpkin, G.R. (1990) Pressure-temperature constraints on the crystallization of the Harding pegmatite, Taos County, New Mexico. Canadian Mineralogist, 28, 287–298.

Dingwell, D.B., Hess, K.U., and Knoche, R. (1996) Granite and granite pegmatite melts: volumes and viscosities. Transactions of the Royal Society of Edinburgh, Earth Sciences, 87, 65–72.

Evensen, J.M. and Meeker, G.P. (1997) Feasibility of Be analysis for geologic materials using EPMA. Microscopy Society of America, Proceedings: Microscopy and Microanalysis 1997, 3, 893–894.

Fleischer, M. and Mandarino, J.A. (1995) Glossary of Mineral Species 1995, 280 p. Mineralogical Record, Tucson, Arizona.

Franz, G. and Morteani, G. (1981) The system BeO-Al_2O_3-SiO_2-H_2O: Hydrothermal investigation of the stability of beryl and euclase in the range from 1 to 6 kb and 400 to 800 °C. Neues Jahrbuch für Mineralogie Abhandlungen, 140, 273–299.

Gan, H. and Hess, P.C. (1989) Phosphorus effects upon the structure of potassium aluminosilicate glass: inference from Raman and NMR. Transactions of the American Geophysical Union (Eos), 70, 1375.

Griffitts, W.R. and Cooley, E.F. (1961) Beryllium content of cordierite. United States Geological Survey Professional Paper 424-B, 259.

Hess, K.U., Dingwell, D.B., and Webb, S.L. (1995) The influence of alkaline-earth oxides (BeO, MgO, CaO, SrO, BaO) on the viscosity of a haplogranite melt: systematics of non-Arrhenian behaviour. European Journal of Mineralogy, 8, 371–381.

Huebner, J.S. (1971) Buffering techniques for hydrostatic systems at elevated pressures. In Research Techniques for High Pressure and High Temperature (G.C. Ulmer, ed.) Springer-Verlag, New York, 123–177.

London, D. (1996) Granitic pegmatites. Transactions of the Royal Society of Edinburgh, Earth Sciences, 87, 305–319.

London, D., Hervig, R.L., and Morgan, G.B. (1988) Vapor-undersaturated experiments with Macusani glass + H_2O at 22 MPa, and the internal differentiation of granitic pegmatites. Contributions to Mineralogy and Petrology, 102, 360–373.

London, D., Morgan, G.B., and Hervig, R.L. (1989) Vapor-undersaturated experiments in the system macusanite-H_2O at 200 MPa. Contributions to Mineralogy and Petrology, 102, 1–17.

Manning, D.A.C., Hamilton, D.L., Henderson, C.M.B., and Dempsey, M.J., (1980) The probable occurence of interstitial Al in hydrous, F-bearing and F-free aluminosilicate melts. Contributions to Mineralogy and Petrology, 75, 257–262.

Morgan, G.B. and London, D. (1989) Experimental reactions of amphibolite with boron-bearing aqueous fluids at 200 MPa: implications for tourmaline stability and partial melting in mafic rocks. Contributions to Mineralogy and Petrology, 102, 281–297.

——— (1996) Optimizing the electron microprobe analysis of hydrous alkali aluminosilicate glasses. American Mineralogist, 81, 1176–1185.

Morgan, G.B., VI, London, D., and Kirkpatrick, R.J. (1990) Reconnaissance spectroscopic study of hydrous sodium aluminum borosilicate glasses. (abstr) Geological Society of America, 22, A167.

Mysen, B. and Virgo, D. (1985) Structure and properties of fluorine-bearing aluminosilicate melts: the system Na_2O-Al_2O_3-SiO_2-F at 1 atm. Contributions to Mineralogy and Petrology, 91, 205–220.

Norton, J.J. and Redden, J.A. (1990) Relations of zoned pegmatites to other pegmatites, granite, and metamorphic rocks in the southern Black Hills, South Dakota. American Mineralogist, 75, 631–655.

Pauling, L. (1960) The Nature of the Chemical Bond, 3rd Ed., 644 p. Cornell University Press, Ithaca, New York.

Pouchou, J.L. and Pichoir, F. (1985) "PAP" (φ−ρ-Z) correction procedure improved quantitative microanalysis. In J.T. Armstrong, Ed., Microbeam Analysis, 104–106. San Francisco Press.

Riebling, E.F. and Duke, D.A. (1967) BeO-Al_2O_3-SiO_2 system: structural relationships of crystalline, glassy, and molten beryl. Journal of Materials Science, 2, 33–39.

Shannon, R.D. (1976) Revised effective ionic radii and systematics studies of interatomic distances in halides and chalcogenides. Acta Crystallographica, 32, 751–767.

Taylor, S.K. (1964) The abundance of chemical elements in the continental crust—a new table. Geochimica et Cosmochimica Acta, 28, 1273–1285.

Toth, L.M., Bates, J.B., and Boyd, G.E. (1973) Raman spectra of Be_2F^{3-} and higher polymers of beryllium fluorides in the crystalline and molten state. Journal of Physics and Chemistry, 77, 216–221.

Tuttle, O.F. and Bowen, N.L. (1958) Origin of granite in the light of experimental studies in the system $NaAlSi_3O_8$-$KAlSi_3O_8$-SiO_2-H_2O. Geological Society of America, Memoir, 74.

Webber, K.L., Falster, A.U., Simmons, W.B., and Foord, E.E. (1997) The role of diffusion-controlled oscillatory nucleation in the formation of line rock in pegmatite-aplite dikes. Journal of Petrology, 38, 1777–1791.

Wuensch, B.J. and Hörmann, P.K. (1978) Beryllium. In K.H. Wedepohl, Ed., Handbook of Geochemistry, Vol. II/1, 4-A-1 to 4-O-1. Springer-Verlag, New York.

MANUSCRIPT RECEIVED AUGUST 10, 1998
MANUSCRIPT ACCEPTED DECEMBER, 12, 1998
PAPER HANDLED BY JAMES G. BLENCOE